Analysis of the Attenuation of Strong Ground Motion on the Island of Hawaii

by Clifford G. Munson[1] and Clifford H. Thurber

Abstract We develop a horizontal peak ground acceleration (PGA) predictive equation for the island of Hawaii by applying the Joyner and Boore (1993, 1994) two-stage regression method to a data set that consists of 51 PGA from 22 events. Magnitudes vary from 4.0 to 7.2, and event depths vary from 4 to 14 km. The resulting equation is

$$\log_{10}\text{PGA} = 0.518 + 0.387 \, (M - 6) - \log_{10}r - 0.00256r + 0.335S,$$

where PGA is measured in units of g, M is magnitude, $r = (d^2 + 11.29^2)^{1/2}$, and S is 0 for lava sites and 1 at ash sites. The distance parameter d is the closest distance from the recording site to the surface projection of the fault rupture area and varies from 0 to 88 km for the Hawaii PGA data set. We find that the attenuation of high-frequency strong ground motion is significantly greater than a previous relationship used for the island of Hawaii. The ash site coefficient S, which represents accelerometer sites with shear-wave velocities that vary from 60 to 200 m/sec, is generally larger than the soil site coefficients in other attenuation relationships.

Introduction

The island of Hawaii has been the site of numerous large earthquakes ($M > 6$) and at least one great earthquake in historic time. Crustal earthquakes in Hawaii ultimately originate from volcanic activity and include both swarms of small-magnitude volcanic events, resulting from magma intrusions beneath or next to Mauna Loa and Kilauea Volcanoes, and larger tectonic events due to stresses exerted on the volcano flanks. These large events result from the growth of rift zone dikes that laterally compress the adjacent flanks of Mauna Loa and Kilauea (Ando, 1979; Crosson and Endo, 1982; Dvorak *et al.*, 1986; Bryan, 1992). Examples of such events include the 1868 $M \approx 8$ great Kau earthquake, the 1975 $M_s = 7.2$ Kalapana earthquake, the 1983 $M_s = 6.6$ Kaoiki earthquake, and the 1989 $M_s = 6.1$ South Flank earthquake. In addition, upper mantle earthquakes, occurring beneath the island at depths greater than about 15 km, result from flexure of the lithosphere under the gravitational load of the island (Klein and Koyanagi, 1989).

The most seismically active flank areas are the south flank of Kilauea and the Kaoiki and Hilea seismic zones located on the southern flank of Mauna Loa (Fig. 1). Focal mechanisms of earthquakes in the Kaoiki and Hilea areas include both near-vertical strike-slip earthquakes (between 4 and 11 km in depth) and low-angle decollement-type earthquakes (between 6 and 12 km in depth) (Endo, 1985). Large events on the south flank of Kilauea, such as the 1975 Kalapana and 1989 South Flank earthquakes, occur along the interface between the top of the prevolcanic sea floor and overlying lava flows (about 9 km in depth) as low-angle thrust events (Crosson and Endo, 1982; Bryan, 1992).

Wyss and Koyanagi (1992) point out that some of the recent destructive earthquakes in Hawaii have not attracted nationwide attention since the loss of property was relatively low. However, major earthquakes have occurred near areas that are now undergoing rapid development such as the Puna and Kau districts. The northeastern part of the island along the Hamakua coast is also growing rapidly (Fig. 1). Much of this region is covered by a thin (≤ 6 m) layer of low-impedance volcanic ash (see Fig. 2) and is therefore susceptible to enhanced ground motion. Seismic wave amplification in these soft soils occurred during the 1973 $M_s = 6.2$ Honomu earthquake, located approximately 10 km north of Hilo, and the 1983 Kaoiki event. Nielson *et al.* (1977) report that most of the damage ($5.6 million) from the 1973 Honomu earthquake, particularly to residential structures, occurred in the ash deposits along the Hamakua coast within a 20-km radius of the epicenter. Structural damage from the 1983 Kaoiki earthquake ($7 million) was also greater in the

[1]Present address: U.S. Nuclear Regulatory Commission, MS: O-7H15, Washington, DC 20555.
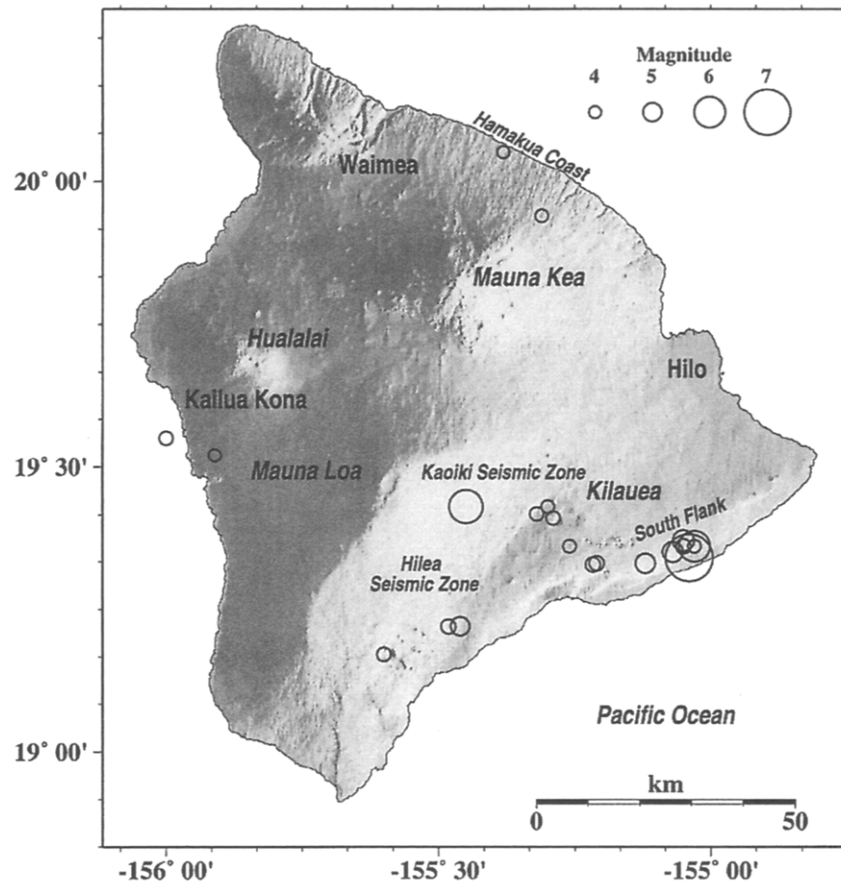
Figure 1.   Shaded relief map of the island of Hawaii showing earthquake locations as circles (scaled by magnitude), population centers, volcanoes, and major fault and rift systems.

areas of the South Hilo District and Wood Valley where buildings are constructed with post-and-pier foundations. During the 1973 Honomu, 1975 Kalapana, and 1983 Kaoiki earthquakes, many of these homes sustained greater structural damage than structures with concrete slab foundations primarily because of lateral displacement of the piers and subsequent decoupling of the piers from the houses (Buchanan-Banks, 1987).

Recent work on seismic hazards in Hawaii includes a catalog of isoseismal maps for earthquakes on the island (Wyss and Koyanagi, 1992) and probabilistic estimates of peak horizontal ground acceleration (PGA) (Klein, 1994). Wyss and Koyanagi (1992) show that the attenuation of seismic waves in the crust is stronger in Hawaii than for other areas of the United States, based on the steeper gradient of isoseismals as a function of epicentral distance for earthquakes in Hawaii. In a plot of magnitude versus maximum intensity, they also show that Hawaii earthquakes have to register at least a unit in magnitude greater than those in California to produce the same maximum intensity. Klein (1994) quantifies the seismic hazard in southern Hawaii by estimating probabilistic PGA as a function of exposure time. The results of his study show that the active flanks of Kilauea

and Mauna Loa can reasonably expect (10% probability of exceedance) a PGA of 1.0 g within an exposure time of 50 yr. Since the Hawaii PGA data set considered by Klein (1994) consists of only 33 PGA from seven Hawaii earthquakes, he does not derive a distinct PGA predictive equation for Hawaii. Instead, Klein uses the Boore et al. (1993) (BJF93) attenuation relationship (class B site term) shifted upward by a factor of 1.2. Klein (1994) uses a modified version of the BJF93 attenuation relationship because it approximates the distance dependence of the Hawaii PGA data set better than six other published peak acceleration predictive equations. However, the BJF93 attenuation relationship is mostly based on California PGA, including 63 PGA from the 1989 $M_w = 6.9$ Loma Prieta earthquake and 95 PGA from the 1992 $M_w = 7.3$ Landers earthquake.

Rather than fitting the Hawaii PGA data set to an existing attenuation relationship, we derive a peak acceleration predictive equation using an expanded data set, 51 PGA from 22 Hawaii earthquakes. We add to the Hawaii PGA data set considered by Klein (1994) by including additional PGA from recent (1993) Hawaii earthquakes and smaller PGA (<0.05 g) not reported in the U.S. Geological Survey (USGS) yearly Strong Motion Program reports. We also
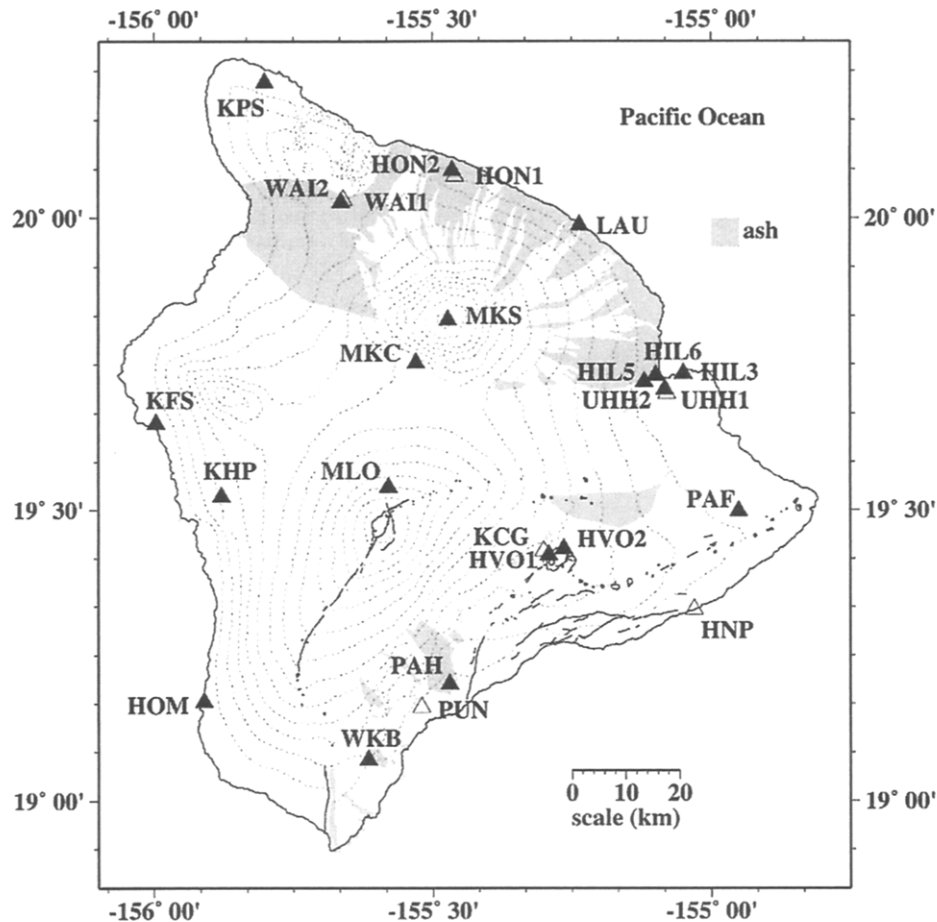
Figure 2.   Current (solid triangles) and previous (open triangles) strong-motion accelerograph sites. Ash deposits are shaded and elevation contours are indicated by dotted lines.

searched the Hawaiian Volcano Observatory (HVO) seismicity catalog to find the locations and magnitudes of six strong-motion records identified in the USGS Strong Motion Program reports only by time intervals between site visits (usually less than 1 yr). To facilitate a comparison to the BJF93 attenuation relationship used by Klein (1994), we use the two-stage regression method of Joyner and Boore (1993, 1994). We find that the attenuation of high-frequency strong ground motion on the island of Hawaii is significantly greater than that for the western United States modeled by the BJF93 attenuation relationship. This difference is accounted for by the inclusion of a geometric spreading coefficient (fixed at −1) together with a negative anelastic attenuation coefficient in the Hawaii attenuation relationship. The BJF93 predictive equation combines these two distance terms since the anelastic attenuation coefficient was initially positive with the geometric spreading coefficient fixed at −1. The greater attenuation on the island of Hawaii, observed by this study and previous studies (Savage, 1987; Scherbaum and Wyss, 1990; Wyss and Koyanagi, 1992), is due to a highly fractured volcanic pile that is less capable of transmitting higher-frequency ground motion than rock in

the western United States. In addition, we find that the ash site term is statistically significant, implying that site geology has a significant effect on PGA on Hawaii. This effect is characterized by large high-frequency reverberations in the thin shallow ash layers that cover large portions of the island and is dramatically illustrated by strong-motion records from the 1983 Kaoiki earthquake recorded at ash sites in Hilo, Waimea, and Honokaa.

Strong-Motion Sites

The Hawaii strong-motion network began in February 1973 when accelerographs were installed in Honolulu, Oahu, and at Hawaii National Park (Porcella, 1983). From 1976 to 1980, the strong-motion network was expanded to include 15 accelerograph stations on the island of Hawaii. Figure 2 shows the locations of current and previous accelerograph sites, and Table 1 lists the station name abbreviations used by this study. All are ground-response stations equipped with Kinemetrics SMA-1 accelerographs. The natural frequency of the SMA-1 is about 25 Hz, and the damping ratio is about 60% of critical (Hudson, 1979). Although

Table 1

Hawaii Strong-Motion Sites

Name	Site
HVO1	Hawaiian Volcano Obs.
HVO2	Hawaiian Volcano Obs. Warehouse
HNP	Wahaula Utility Center
UHH1,2	UH-Hilo (Cloud Physics Lab., Wentworth Hall)
HIL3	Hilo Sewage Treatment Center
HIL5	Hilo USDA Lab (formerly U.S. Fish and Wildlife)
HIL6	Old Hilo Hospital
HOM	Honomalino (MacFarms)
HON1,2,3	Honokaa (Central Service Bldg., High School, Police Station)
KCG	Kilauea Camp Ground
KFS	Kailua Kona Fire Station
KPS	Kohala Kapaau Police Station
KHP	Kona Hospital (Kealakekua)
LAU	Laupahoehoe Post Office
MKC	Mauna Kea Visitor Center
MKS	Mauna Kea Summit
MLO	Mauna Loa NOAA Obs.
PAH	Pahala Kau Hospital
PAF	Pahoa Fire Station
PUN	Punaluu Village Service Bldg.
WAI1,2	Waimea (School, Fire Station)
WKB	Waiohinu Kau Baseyard

the majority of accelerograph sites are located on lava, there are currently four stations located on volcanic ash in Hilo, Honokaa, Waimea, and Pahala.

Volcanic ash deposits are air-fall deposits erupted mainly from Mauna Kea Volcano, with minor contributions from Mauna Loa and Kilauea (Wieczorek *et al.*, 1982; Rubin *et al.*, 1987). The ash consists of weathered, weakly cemented, fine particles of volcanic glass (Wieczorek *et al.*, 1982). The ash near Hilo has a high water content due to high rainfall in the area and the water-retentive properties of the ash (Buchanan-Banks, 1983). Nielsen *et al.* (1977) report a density of 0.95 to 1.30 g/cm^3 for the ash deposits along the Hamakua coast.

Since no seismic or geotechnical properties have been measured for Hawaii strong-motion sites (Maley, personal comm., 1994), during the summer of 1994, we collected seismic refraction data at four ash sites using both vertical- and horizontal-component geophones with 10- to 15-ft spacing, a 12-channel seismograph, and a 4.5-kg hammer as an energy source. To estimate near-surface seismic velocities, we used the forward-modeling program MacRay (Luetgert, 1992). Measured S-wave velocities at the three Hamakua coast ash sites (HIL5, WAI2, and HON2) increase from 60 to 100 m/sec near the surface to approximately 200 m/sec at a depth of 3 to 5 m. We measured an S-wave velocity of 200 m/sec for the Pahala site (PAH) but were unable to estimate a layer thickness. Wieczorek *et al.* (1982) state that the maximum ash thickness is 17 m near Pahala, and Buchanan-Banks (1983) reports a maximum ash thickness of 6 m in the Hilo area.

Significant Strong-Motion Records

1975 Kalapana Earthquake

The 29 November 1975 $M_s = 7.2$ Kalapana earthquake is the most damaging earthquake to occur on the island of Hawaii since the great Kau earthquake ($M \approx 8$) in 1868. The mainshock was preceeded by an $M_L = 5.7$ foreshock and produced a tsunami that reached a height of almost 15 m above sea level (Tilling *et al.*, 1976). The hypocenter of the earthquake was located on the south flank of Kilauea Volcano at a depth of approximately 9 km (Fig. 3). Aftershocks occurred over an area 40 km in length and 5 km wide. Three SMA-1 instruments triggered on both the foreshock and mainshock. The closest strong-motion site to the epicenter (40 km), located on the campus of the University of Hawaii-Hilo (UHH1), recorded a peak acceleration of 0.22 g. Harvey and Wyss (1986), using strong-motion synthetics, model the mainshock as a sequence of six major subevents propagating away from station UHH1 toward Punaluu (PUN). This direction of propagation is based on the different appearances of the two accelerograms, as shown in Figure 3. At station UHH1, the six subevents are separated by 5 to 10 sec over a 55-sec time interval, while at PUN, the subevents occur over a 20-sec interval. They conclude that the rupture stopped between subevents since dividing the rupture length (40 km) by the duration of strong ground shaking (≈ 50 sec) results in a rupture velocity of only 0.8 km/sec, (about 25% of the S-wave velocity).

1983 Kaoiki Earthquake

The 16 November 1983 $M_s = 6.6$ Kaoiki earthquake occurred in an area of high seismicity between Mauna Loa and Kilauea Volcanoes. The earthquake caused considerable damage to the southeastern part of the island and is the largest to occur in the Kaoiki region in more than a century (Koyanagi *et al.*, 1984; Chiu *et al.*, 1984). The earthquake produced surface ruptures that extend over a distance of 6 km within the Kaoiki seismic zone (Jackson *et al.*, 1992). Horizontal PGA near the epicentral region vary from 0.87 g at the Hawaiian Volcano Observatory (HVO) to 0.58 g near the summit of Mauna Loa (MLO). Reports following this event considered the PGA of 0.87 g recorded at the HVO site to be due to a high-frequency pulse superimposed on the main pulse of the record, and as such, they reduce the PGA to 0.67 g (Koyanagi *et al.*, 1984; Buchanan-Banks, 1987). However, this supposition was never confirmed (Klein, personal comm., 1997), and a later study by Wyss and Koyanagi (1992) re-establishes a PGA of 0.87 g for the HVO site. Figure 4 shows the larger horizontal component of acceleration for the 15 stations that recorded this event. Accelerations at ash sites along the Hamakua coast (HIL5 and HON2) are dramatically enhanced at high frequencies compared to nearby lava sites (HIL3 and UHH2). A comparison of the lava (Fig. 5a) and ash (Fig. 5b) acceleration response spectra (5% damping) clearly shows that ash deposits may significantly increase the amplitude of shaking in narrow-fre-
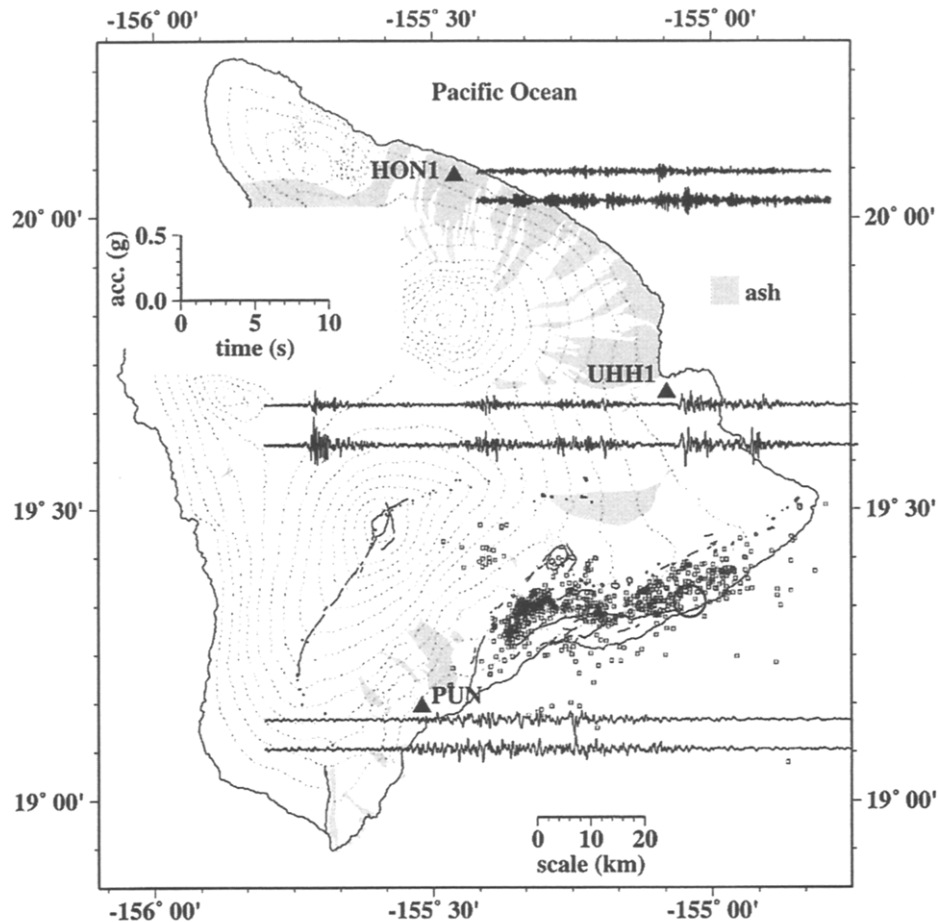
Figure 3. Accelerograms from the 1975 $M_s = 7.2$ Kalapana mainshock overlain on a map showing station locations (triangles) and aftershocks (squares) for a 7-day period following the mainshock (circle). Shown are the two horizontal components in the directions as originally recorded.

quency bands. The predominant frequency of the accelerograms recorded at HON2 and WAI2 is shown by the peak of their respective response spectra near 10 Hz, while the HIL5 response spectrum shows a predominant frequency near 3 Hz. The higher resonance frequencies for the Honokaa (HON2) and Waimea (WAI2) sites imply a thinner ash layer than for the Hilo (HIL5) and Pahala (PAH) sites.

1989 South Flank Earthquake

The 26 June 1989 $M_s = 6.1$ South Flank earthquake occurred along the northern end of the Hilina fault system at a depth of 9 km (Koyanagi *et al.*, 1989; Bryan, 1992). Damage resulting from this event was focused in the Kalapana area of Kilauea's south flank. This event appears to have consisted of two separate subevents about 5 sec apart. Fourteen strong-motion stations at epicentral distances ranging from 20 to 106 km were triggered. Records at PAH, HIL6, and UHH2 triggered on the first subevent *P*-wave arrival and thus include the subsequent *S*-wave arrival as well as *P*- and *S*-wave arrivals from the second subevent (Fig. 6). Bryan (1992) identifies a zone of relatively high

aftershock activity located approximately 12 km east of the hypocenter and postulates that this zone may define an area of secondary rupture. Peak accelerations near 0.20 *g* were recorded at Pahoa (an epicentral distance of 20 km) and at an ash site in Hilo (an epicentral distance of 44 km). Despite epicentral distances of about 20 km, peak accelerations at Hawaiian Volcano Observatory stations HVO1 and HVO2 only reached 0.05 *g*. The relatively weak ground motions at these two sites may result from the possible combination of source effects (radiation pattern and directivity) and a travel path through the highly fractured south flank and caldera of Kilauea.

Data

For this study, the PGA data set consists of 51 measurements from 22 Hawaii earthquakes (Table 2). Magnitudes vary from 4.0 to 7.2, and event depths vary from 4 to 14 km. For peak acceleration values, we use the larger of the two horizontal components in the directions as originally recorded. The moment magnitude, M_w, of Hanks and Kan-

Table 2
Hawaii PGA Data Set

Date	Ep. Region	M	CD†	Station	Lat.	Long.	S	PGA (g)
5 May 74	South Flank	4.3	9	KCG	19.430	−155.300	L	0.05
29 Nov 75	South Flank	5.7	35	UHH1	19.700	−155.080	L	0.15
29 Nov 75	South Flank	5.7	55	PUN	19.160	−155.520	L	0.03
29 Nov 75	South Flank	5.7	86	HON1	20.070	−155.460	A	0.06
29 Nov 75	South Flank	7.2	22	UHH1	19.700	−155.080	L	0.22
29 Nov 75	South Flank	7.2	33	PUN	19.160	−155.520	L	0.12
29 Nov 75	South Flank	7.2	79	HON1	20.070	−155.460	A	0.09
*23 Dec 75	Kilauea	4.2	0	KCG	19.430	−155.300	L	0.05
*15 Jan 76	Kilauea	4.4	2	KCG	19.430	−155.300	L	0.06
*20 Apr 77	Hamakua Coast	4.3	23	HON2	20.080	−155.470	A	0.07
*2 May 77	Hamakua Coast	4.0	10	HON2	20.080	−155.470	A	0.06
21 Sep 79	South Flank	5.5	3	HNP	19.329	−155.031	L	0.09
*20 Mar 83	South Flank	4.9	2	HNP	19.329	−155.031	L	0.12
*9 Sep 83	South Flank	5.4	9	HNP	19.329	−155.031	L	0.06
16 Nov 83	Kaoiki	6.6	2	HVO1	19.423	−155.291	L	0.87
16 Nov 83	Kaoiki	6.6	12	MLO	19.539	−155.580	L	0.58
16 Nov 83	Kaoiki	6.6	29	MKC	19.752	−155.530	L	0.26
16 Nov 83	Kaoiki	6.6	31	HNP	19.329	−155.031	L	0.12
16 Nov 83	Kaoiki	6.6	33	WKB	19.070	−155.620	L	0.19
16 Nov 83	Kaoiki	6.6	39	PAF	19.498	−154.950	L	0.18
16 Nov 83	Kaoiki	6.6	39	UHH2	19.707	−155.083	L	0.11
16 Nov 83	Kaoiki	6.6	40	KHP	19.523	−155.879	L	0.10
16 Nov 83	Kaoiki	6.6	43	HIL3	19.734	−155.050	L	0.10
16 Nov 83	Kaoiki	6.6	56	KFS	19.649	−155.996	L	0.04
16 Nov 83	Kaoiki	6.6	88	KPS	20.230	−155.801	L	0.09
16 Nov 83	Kaoiki	6.6	15	PAH	19.200	−155.470	A	0.59
16 Nov 83	Kaoiki	6.6	40	HIL5	19.731	−155.100	A	0.50
16 Nov 83	Kaoiki	6.6	62	WAI2	20.030	−155.060	A	0.13
16 Nov 83	Kaoiki	6.6	64	HON3	20.080	−155.465	A	0.37
21 Feb 85	South Flank	4.8	13	HVO1	19.423	−155.291	L	0.05
7 Jul 85	Hilea	4.4	11	WKB	19.070	−155.620	L	0.10
12 Dec 85	Kona Coast	4.0	3	KHP	19.523	−155.879	L	0.03
9 Jul 86	Kona Coast	4.6	8	KHP	19.523	−155.879	L	0.14
20 Feb 88	South Flank	4.2	3	HNP	19.329	−155.031	L	0.04
2 Mar 88	South Flank	4.9	13	HVO1	19.423	−155.291	L	0.03
4 Jul 88	Hilea	5.2	20	WKB	19.070	−155.620	L	0.16
4 Jul 88	Hilea	5.2	28	HVO1	19.423	−155.291	L	0.03
4 Jul 88	Hilea	5.2	0	PAH	19.200	−155.470	A	0.15
26 Jun 89	South Flank	6.1	17	PAF	19.498	−154.950	L	0.21
26 Jun 89	South Flank	6.1	33	HVO2	19.434	−155.264	L	0.05
26 Jun 89	South Flank	6.1	35	HVO1	19.423	−155.291	L	0.05
26 Jun 89	South Flank	6.1	40	UHH2	19.707	−155.083	L	0.11
26 Jun 89	South Flank	6.1	44	HIL3	19.734	−155.050	L	0.07
26 Jun 89	South Flank	6.1	41	HIL6	19.720	−155.120	A	0.20
26 Jun 89	South Flank	6.1	45	PAH	19.200	−155.470	A	0.05
25 Jan 93	Kilauea	4.4	2	HVO1	19.423	−155.291	L	0.10
26 Jan 93	Hilea	4.8	21	WKB	19.070	−155.620	L	0.04
26 Jan 93	Hilea	4.8	1	PAH	19.200	−155.470	A	0.28
8 Jun 93	South Flank	4.9	12	HVO2	19.434	−155.264	L	0.03
8 Jun 93	South Flank	4.9	13	HVO1	19.423	−155.291	L	0.05
8 Jun 93	South Flank	4.9	30	PAH	19.200	−155.470	A	0.06

†Closest distance (km).
*Record and event association made by authors.

amori (1979) is used by Joyner and Boore for their peak acceleration predictive relationships. However, since M_w are not available for a majority of Hawaii earthquakes, we use M_s for the three large events (1975 Kalapana mainshock, 1983 Kaoiki, and 1989 South Flank) and M_L, as determined by HVO (Tomori *et al.*, 1991), for the remaining events. To differentiate between the large tectonic earthquakes occurring on the flanks of Mauna Loa and Kilauea Volcanoes and the deeper mantle events occurring beneath the island, we use a depth cutoff of 15 km. The average depth of the 22 earthquakes that comprise the Hawaii PGA data set is 9.6 km with a standard deviation of 2.3 km. The distance mea-
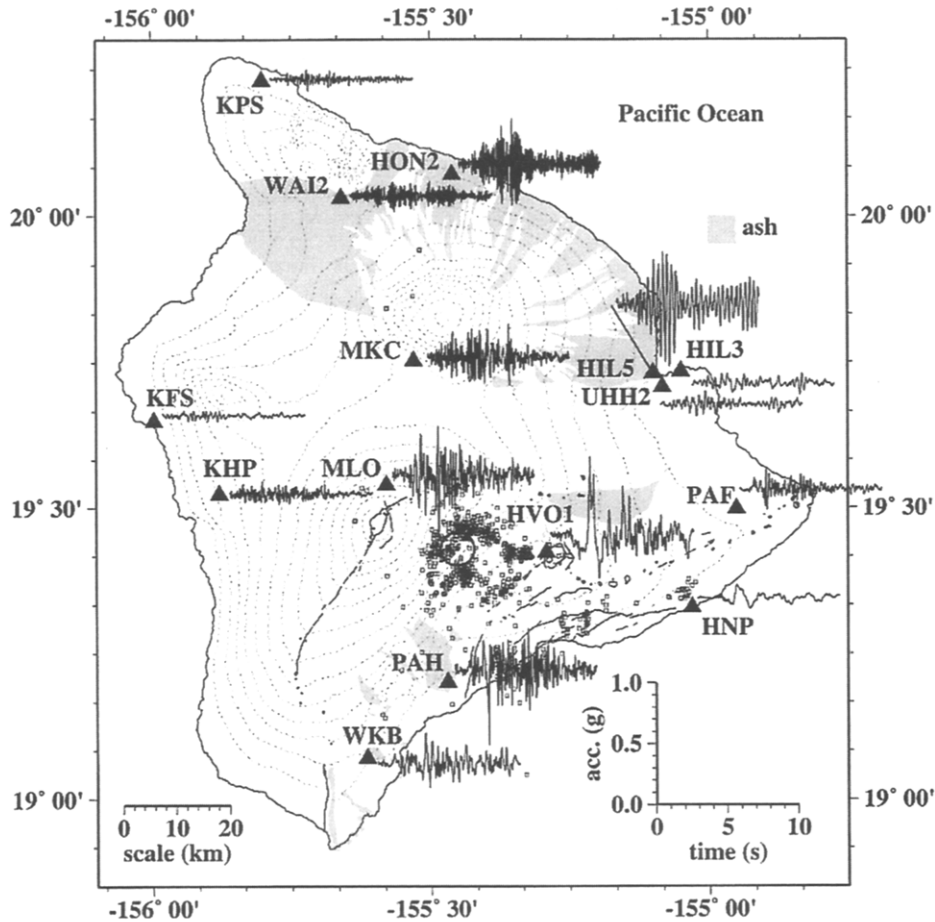
Figure 4.   Accelerograms from the 1983 M_s = 6.6 Kaoiki earthquake overlain on a map showing station locations (triangles) and aftershocks (squares) for a 7-day period following the mainshock (circle). Shown are the larger of the two horizontal components for each station in the directions as originally recorded.

sure used by the Joyner and Boore regression method is the closest distance from the recording site to the surface projection of the slipped fault. For each earthquake, we used an outline of the aftershock zone to approximate the fault rupture area. Figure 7 shows the distribution of the PGA data set for lava and ash sites as a function of magnitude and closest distance to the surface projection of the slipped fault.

We use peak acceleration values scaled directly from the Hawaii strong-motion records rather than PGA from processed records. To validate our decision to use PGA values from the unprocessed accelerograms, we digitized a number of Hawaii strong-motion records provided to us by the USGS National Strong-Motion Program. Prior to this study, the only digitized Hawaii strong-motion records were four records from the 1975 Kalapana foreshock and mainshock and 15 records from the 1983 Kaoiki earthquake. After digitization, we did not apply a correction for the instrument characteristics because reliable values of the natural frequency and damping ratio are not available for the majority of the records. However, for the SMA-1 accelerograph, the instrument characteristics only significantly distort the recorded

amplitude at frequencies greater than about 25 Hz (Hudson, 1979). To reduce noise in the low- and high-frequency ranges, we applied a bandpass filter with corner frequencies of 0.1 and 25 Hz to the accelerograms. The resulting peak accelerations do not diminish by more than 0.05 g for the larger ground-motion records (PGA $\geqq$ 0.20 g) compared to the peak accelerations scaled directly from the unprocessed accelerograms. For the smaller ground-motion records, there was little or no difference between the PGA from the processed and unprocessed accelerograms.

Since the installation of the first strong-motion accelerograph in 1973, 175 records collected from sites on the island have not been attributed, in the annual USGS National Strong-Motion Program reports, to a particular event. This large number of unidentified records is due to the high seismicity of the island and also to the length of time between site maintenance visits. Of the 175 unidentified records, 42% are from sites located on volcanic ash, and 27% are from sites located in regions of high seismicity (Kilauea caldera and south flank). Most of the PGA from these records are less than 0.05 g, but there are 35 records (20%) with PGA
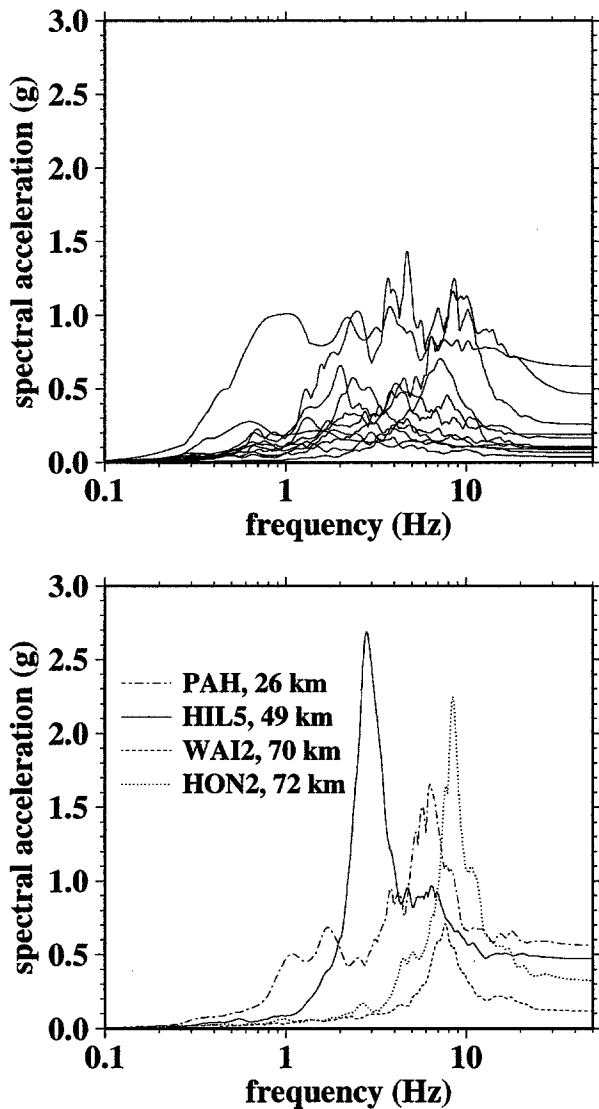
Figure 5. Lava (top) and ash (bottom) response spectra (5% damping) from the larger horizontal component accelerograms of the 1983 Kaoiki M_s = 6.6 earthquake. The frequency content of the ash site ground motion is shown by large spectral acceleration peaks near 10 Hz for Waimea (WAI2) and Honokaa (HON2) and 3 Hz for Hilo (HIL5).

$\geqq$ 0.05 g. By examining the HVO seismicity catalog for the site-maintenance time periods associated with each unidentified record, we were able to find locations and magnitudes for six records, which are identified by an asterisk in Table 2. The two criteria for attributing these records to events in the HVO catalog are (1) the close proximity of a relatively large magnitude event and (2) the absence of other comparably sized events near the recording site during the time period.

The two-stage regression method developed by Joyner and Boore for attenuation relationships calls for the elimination of records from instruments triggered by the S-wave arrival, since the strongest motion may have been missed,

and also the elimination of records that fall outside of a "distance cutoff." The distance cutoff is defined by Joyner and Boore as the distance to an operational *nontriggered* instrument (Joyner and Boore, 1981) and is imposed to avoid any bias arising from the exclusion of low values of ground motion. We eliminated 3 PGA from consideration due to an instrument triggered by an S-wave arrival and 29 PGA due to the distance cutoff requirement. Table 3 lists the cutoff distances for each event, the operational nontriggered instrument, and the subsequent records that were excluded.

Analysis Method and Results

We use the Joyner and Boore (1993, 1994) two-stage regression method designed to decouple the distance dependence from the magnitude dependence. In the first stage, the distance dependence is determined along with a set of amplitude factors, P_i, for each earthquake, E_{ni}. The first stage, as applied to the Hawaii PGA data set, is given by

$$Y_n = P_i E_{ni} + b_2 r_n + b_3 \log_{10} r_n + b_4 S_n + \varepsilon_r, \quad (1)$$

where $Y_n = \log_{10} \text{PGA}_n$, $E_{ni} = 1$ if recording n comes from earthquake i and 0 otherwise, $S_n = 1$ for ash sites and 0 otherwise, $r_n = (d_n^2 + h^2)^{1/2}$, and ε_r is the error term. With the coefficient b_3 set equal to -1 to account for geometrical spreading, the term $b_2 r_n$ characterizes the effects of anelastic attenuation (material damping and scattering). The variable d_n is the closest distance from the recording site n to the surface projection of the fault rupture area. The variable h is a "fictitious" depth parameter and is introduced to allow for the possibility that the source of the peak acceleration is from a high stress zone on the fault rupture surface rather than the edge or closest point on the rupture (Joyner and Boore, 1981). However, since the location of this high stress zone for each of the earthquakes is unknown, Joyner and Boore solve for estimates of the other parameters in the first regression stage ($\hat{P}$, $\hat{b}_2$, $\hat{b}_4$, and the estimated variance of ε_r, s_r^2) for trial values of h. The value of h that minimizes the residual sum of squares (RSS), is determined iteratively. As shown in Figure 8, the value of h that minimizes the misfit for the Hawaii PGA data set is 11.29 km.

For the second stage, the amplitude factors are regressed against magnitude to determine the magnitude dependence

$$\hat{P}_i = b_0 + b_1 (M_i - 6) + \varepsilon_e, \quad (2)$$

where M_i is the magnitude and ε_e is the error term. Joyner and Boore (1994) use a diagonal weighting matrix, $\mathbf{V}$, given by

$$V_i = (\sigma_r^2/R_i + \sigma_e^2), \quad (3)$$

where R_i is the number of recordings for each earthquake i and σ_e^2 is the variance of ε_e. The least-squares solution for the parameter vector $\mathbf{B}$ is given by
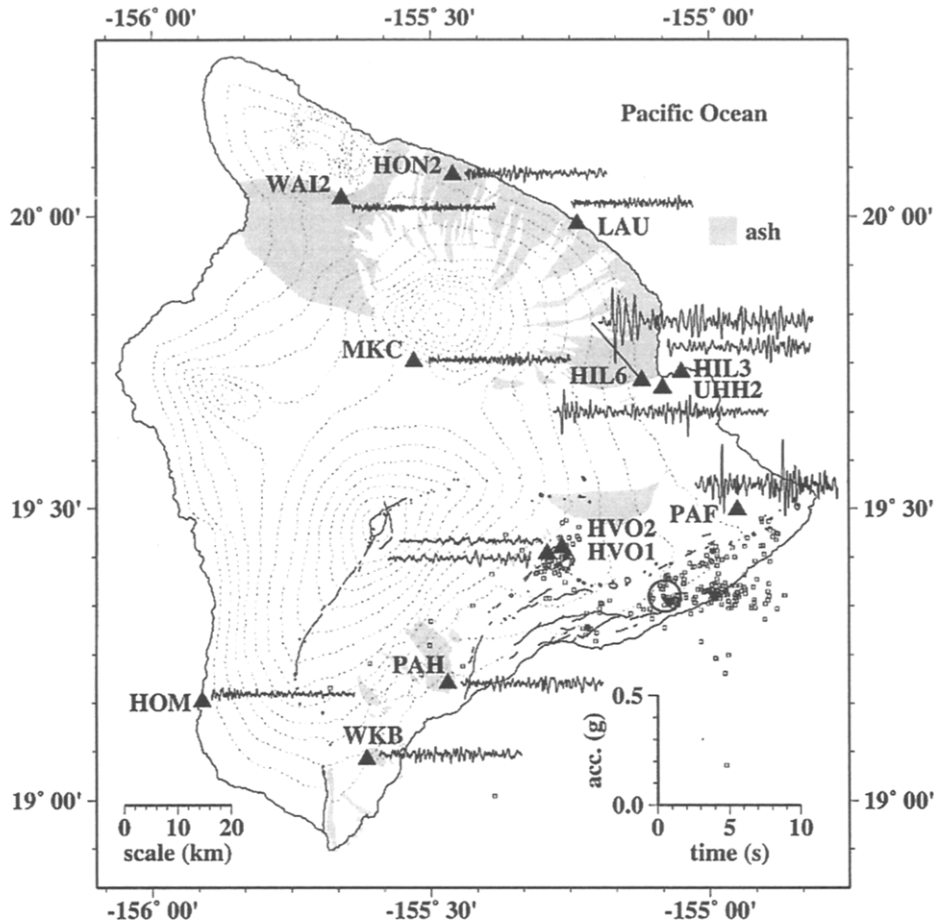
Figure 6. Accelerograms from the M_s = 6.1 1989 South Flank earthquake overlain on a map showing station locations (triangles) and aftershocks (squares) for a 7-day period following the mainshock (circle). Shown are the larger of the two horizontal components for each station in the directions as originally recorded.

$$\mathbf{B} = (\mathbf{X}^T\mathbf{V}^{-1}\mathbf{X})^{-1}\mathbf{X}^T\mathbf{V}^{-1}\mathbf{Y}, \qquad (4)$$

where

$$\mathbf{Y} = \begin{bmatrix} \hat{P}_1 \\ \hat{P}_2 \\ \vdots \\ \hat{P}_N \end{bmatrix},$$

$$\mathbf{B} = \begin{bmatrix} b_0 \\ b_1 \end{bmatrix},$$

and

$$\mathbf{X} = \begin{bmatrix} 1 & M_1 - 6 \\ 1 & M_2 - 6 \\ \vdots & \vdots \\ 1 & M_N - 6 \end{bmatrix}.$$

Since σ_e^2 is unknown, Joyner and Boore (1993) determine its value by estimating the expected value of RSS given by

$$E[(\mathbf{Y} - \mathbf{X}\mathbf{B})^T\mathbf{V}^{-1}(\mathbf{Y} - \mathbf{X}\mathbf{B})] = N - 2, \qquad (5)$$

where E denotes expectation and $N - 2$ is the number of degrees of freedom. Trial values of σ_e^2 are first inserted in equations (3) and (4) to obtain values for $\mathbf{V}$ and $\mathbf{B}$ that are then substituted into equation (5). The value of σ_e^2 that most nearly satisfies equation (5) is determined iteratively with zero as the starting value.

Figure 9 is a plot of the amplitude factors, P_i, as a function of the predictor variable $M_i - 6$. The size of each point is proportional to its corresponding weight determined by the number of records for each event. Thus, the 1983 Kaoiki earthquake (15 records) and the 1989 South Flank earthquake (7 records) receive the most weight. Also shown are the weighted (solid line) and unweighted (dashed line) straight-line fits to the data. Using weighted least-squares instead of ordinary least-squares estimation results in a smaller estimate of σ_e (0.063 versus 0.192). The size of the slope, shown in Figure 9, determines the magnitude dependence of the peak acceleration predictive relationship.
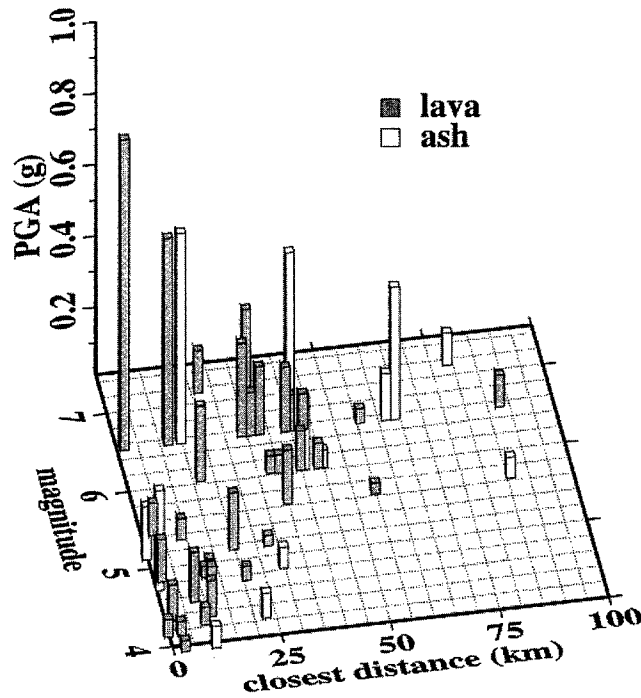
Figure 7. Hawaii PGA values as a function of magnitude and closest distance to the surface projection of the fault rupture area.

The final peak acceleration predictive relationship is then given by

$$Y_n = b_0 + b_1 (M_i - 6) + b_2 r_n$$
$$+ b_3 \log_{10} r_n + b_4 S_n + \varepsilon_r + \varepsilon_e, \quad (6)$$

and the overall variance, σ_Y^2, is given by combining the variances from the two regression stages:

$$\sigma_Y^2 = \sigma_r^2 + \sigma_e^2. \quad (7)$$

The regression coefficients for the Hawaii PGA predictive relation are given in Table 4 along with the uncertainty estimates s_r, s_e, and s_Y.

In performing the regression analysis, we have assumed that the residuals are independent, have a constant variance, and follow a normal distribution. To test these assumptions, we constructed a normal probability plot of the residuals (Fig. 10a), a plot of the residuals against the fitted values $\hat{Y}$ (Fig. 10b), and a plot of the residuals against the two independent variables magnitude and distance (Figs. 10c and 10d). For each of the bivariate residual plots, we distinguish between PGA recorded on ash and lava sites. As shown in Figure 10a, the residuals appear to be normally distributed since the points on the normal probability plot lie approxi-

Table 3

Event Cutoff Distances, Nontriggered Station, and Excluded Records

Date	M	CD*	Station†	Excluded Records
5 May 74	4.3	—	—	—
29 Nov 75	5.7	—	—	—
29 Nov 75	7.2	—	—	—
23 Dec 75	4.2	—	—	—
15 Jan 76	4.4	—	—	—
20 Apr 77	4.3	—	—	—
2 May 77	4.0	—	—	—
21 Sep 79	5.5	20	PAF	UHH2, HIL3, HIL5, PAH, HON3
20 Mar 83	4.9	—	—	—
9 Sep 83	5.4	25	PAF	HIL5
16 Nov 83	6.6	—	—	—
21 Feb 85	4.8	19	HNP	HIL5, PAH
7 Jul 85	4.4	—	—	—
12 Dec 85	4.0	—	—	—
9 Jul 86	4.6	—	—	—
20 Feb 88	4.2	—	—	—
2 Mar 88	4.9	19	HNP	PAH
4 Jul 88	5.2	—	—	—
26 Jun 89	6.1	55	MLO	MKC, MKS, LAU, WKB, WAI2, HON3, HOM
25 Jan 93	4.4	—	—	—
26 Jan 93	4.8	30	HVO	HOM, KHP, HON3
8 Jun 93	4.9	34	PAF	HIL5, KHP, MKC, MKS, MLO

*Cutoff distance (km).
†Nontriggered station.

Table 4

Parameter Estimates

Parameter	Estimate	n	Mean	S.D.	50th	16th	84th
b_0	0.518	100	0.512	0.276	0.517	0.338	0.711
b_1	0.387	100	0.392	0.052	0.392	0.332	0.449
b_2	-0.00256	78	-0.004	0.003	-0.004	-0.007	-0.001
b_3	-1						
b_3*		22	-0.875	0.182	-0.936	-1.069	-0.674
b_4	0.335	100	0.348	0.079	0.343	0.271	0.434
h	11.29	100	12.35	7.52	11.40	5.97	16.83
σ_r	0.228						
σ_e	0.063						
σ_Y	0.237	100	0.249	0.029	0.246	0.222	0.277

*For 1st stage simulations resulting in $+b_2$.
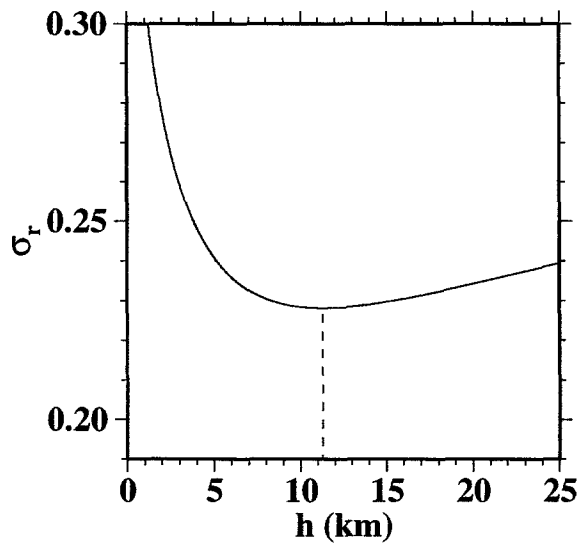
Figure 8. Misfit (σ_r) as a function of the fictitious depth parameter h for the first regression stage. The minimum value of $\sigma_r(h)$ is indicated by a vertical line.
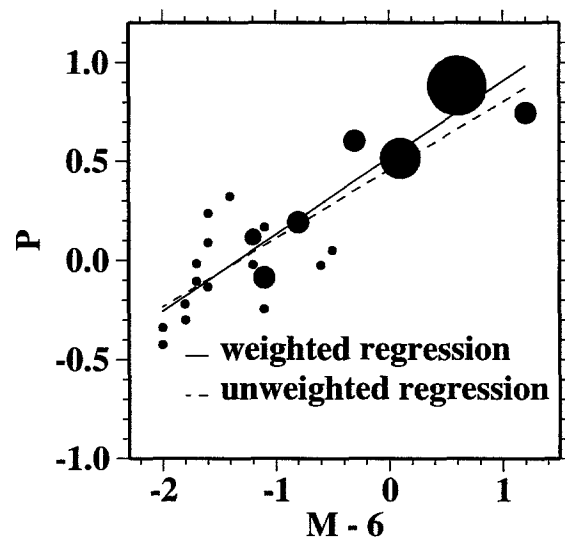
Figure 9. Amplitude factor $(\hat{P})$, from the first regression stage, as a function of magnitude for weighted (solid line) and unweighted (dashed line) second-stage regression equations.

mately in a straight line. The results of the Anderson–Darling test (see Snedecor and Cochran, 1994) also confirm our normal distribution assumption for the residuals since the Anderson–Darling statistic, $A^2_{51,0.05} = 0.295$, is less than the upper 0.05 percentile of this statistic for a sample size of 51, $A^2_{51,0.05} = 0.733$. In addition, each of the residual plots (Figs. 10b through 10d) show a "horizontal band" appearance (see Draper and Smith, 1981), thereby confirming that the residuals are independent and have a constant variance. The Joyner and Boore regression method assumes a magnitude-independent shape because this model requires fewer parameters (Joyner and Boore, 1981). This assumption is confirmed by the absence of any trend for the residual versus magnitude plot shown in Figure 10c.

Since the Joyner and Boore two-stage regression method uses a nonlinear model, Monte Carlo simulation must be used to estimate the parameter uncertainties. Simulated PGA values are obtained by applying the parameter

estimates $\hat{b}_{0-4}$ and h, determined from the actual data set, together with the magnitude, distance, and site values to equation (6). Values for ε_r and ε_e are obtained by a separate random sampling of the two normal distributions $N(0,\sigma_r^2)$ and $N(0,\sigma_e^2)$. We applied the Joyner and Boore method to 100 simulated data sets. Table 4 gives the mean, standard deviation, median, 16th, and 84th percentile values for each model parameter. For 22 of the 100 runs, we obtained a positive value for the anelastic attenuation coefficient, b_2, with b_3 fixed at -1 to account for geometric spreading. For these 22 runs, we then set $b_2 = 0$ and solved for the coefficient b_3 instead, thereby combining the geometric spreading and anelastic attenuation terms. As a result, Table 4 gives parameter uncertainties for b_2 for 78 runs and for b_3 for the other 22 runs. As shown in Table 4, the largest amount that a mean parameter value from the simulations differs from the actual data set parameter estimate is less than one standard deviation from the mean.
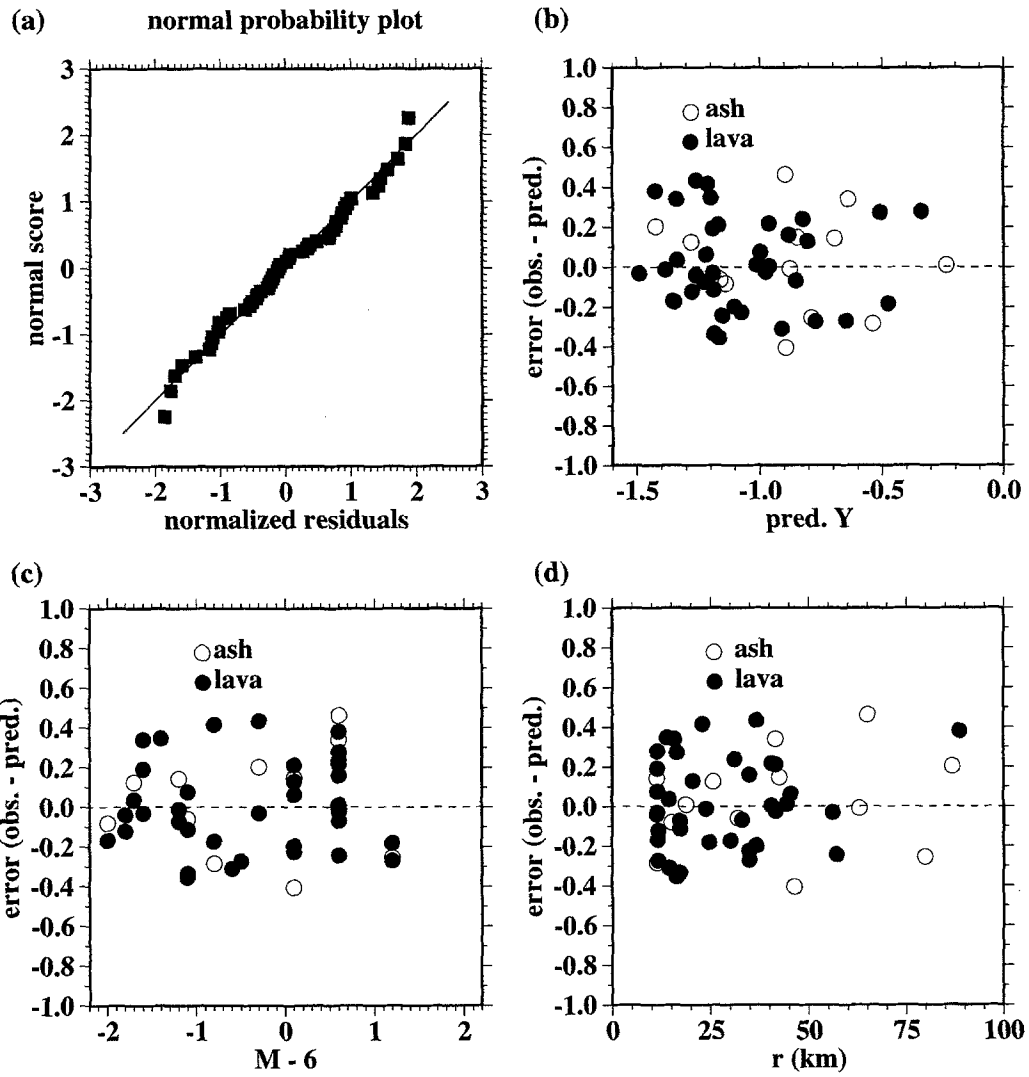
Figure 10.   (a) Normal probability plot of residuals from PGA attenuation relationship. Bivariate residual plots for (b) $\hat{Y}$, (c) magnitude, and (d) the distance parameter r.

Table 5
PGA Predictions

M	CD (km)	($\hat{Y}$)	PGA (g)	mean $\hat{Y}$	PGA (g)	S.D. $\hat{Y}$
7.0	0	−0.176	0.67	−0.148	0.71	0.192
6.0	0	−0.563	0.27	−0.540	0.29	0.157
5.0	0	−0.950	0.11	−0.931	0.12	0.135
7.0	20	−0.515	0.31	−0.524	0.30	0.090
6.0	20	−0.902	0.13	−0.915	0.12	0.060
5.0	20	−1.290	0.05	−1.307	0.05	0.067
7.0	40	−0.820	0.15	−0.817	0.15	0.066
6.0	40	−1.207	0.06	−1.209	0.06	0.058
5.0	40	−1.594	0.03	−1.601	0.03	0.088

Table 5 shows the predicted value of Y, $\log_{10}$ PGA, for magnitudes of 5.0, 6.0, and 7.0 at closest distances of 0, 20, and 40 km. We also determined the mean and standard deviation of $\hat{Y}$ for these magnitudes and distances using the parameter estimates obtained from each of the 100 simulations. The results for a closest distance of 0 km and a magnitude of 7.0 show a small negative bias (-0.04 g) in the predictions. This bias is expected because there are few data points near this magnitude and distance combination. For $M = 7.0$ at 20 and 40 km and $M = 5.0$ and 6.0 at the three distances 0, 20, and 40 km, there is very little or no difference between $\hat{Y}$ as determined from the mean of the simulated parameter estimates and $\hat{Y}$ as determined from the actual parameter estimates. Joyner and Boore (1993) point out that the standard deviation of $\hat{Y}$, resulting from the simulated parameter estimates, represents the contribution to prediction error from stochastic uncertainty in the parameters. The standard deviations shown in Table 5 for the combinations of the magnitudes and distances is less than the Monte Carlo simulation value of σ_Y, as given by equation (7), indicating that σ_Y does not underestimate the total prediction error.

Comparison of Attenuation Relationships

The difference in the attenuation relationship developed in this study and the relationship used by Klein (1994) for his seismic hazard study is illustrated in Figure 11a. Although the attenuation curve used by Klein (1994) is within one standard deviation of the curve developed in this study, the overall shapes of the two curves are quite different. This difference is due to the inclusion of two distance terms, $b_2 r$ and $b_3 \log_{10} r$ with $\hat{b}_2 = -0.00256$ and $b_3 = -1$, in our attenuation relationship that in combination lead to smaller peak accelerations beyond a distance of 20 km. The BJF93 relationship, used by Klein (1994), eliminates the $b_2 r$ term since b_2 was positive with b_3 fixed at -1 to account for geometric spreading. The final value of b_3 for their curve is -0.777. For a direct comparison to the BJF93 attenuation rate, we set $b_2 = 0$ in the first regression stage and solved for b_3, obtaining $\hat{b}_3 = -1.402$.

As a result of shifting the BJF93 attenuation relationship (class B site term) upward by a factor of 1.2, the Klein (1994) relationship predicts larger PGA over the magnitude range from 4.0 to 6.5 and at small distances ($d \leq 10$ km) than the attenuation relationship developed in this study. For example, for $M = 6$ and $d = 0$ km, the PGA predicted by Klein is 0.42 g versus a predicted PGA of 0.27 g from our attenuation relationship. This difference is also illustrated in Figure 11 for $M = 6.6$. The two relationships predict similar PGA for larger-magnitude events ($7.0 \leq M \leq 7.2$) at $d = 0$; however, due to few values in the Hawaii PGA data set, predicted PGA values for these magnitude and distance combinations are not well constrained.

The BJF93 site classes C and D represent sites with average S-wave velocities from 180 to 360 m/sec and less
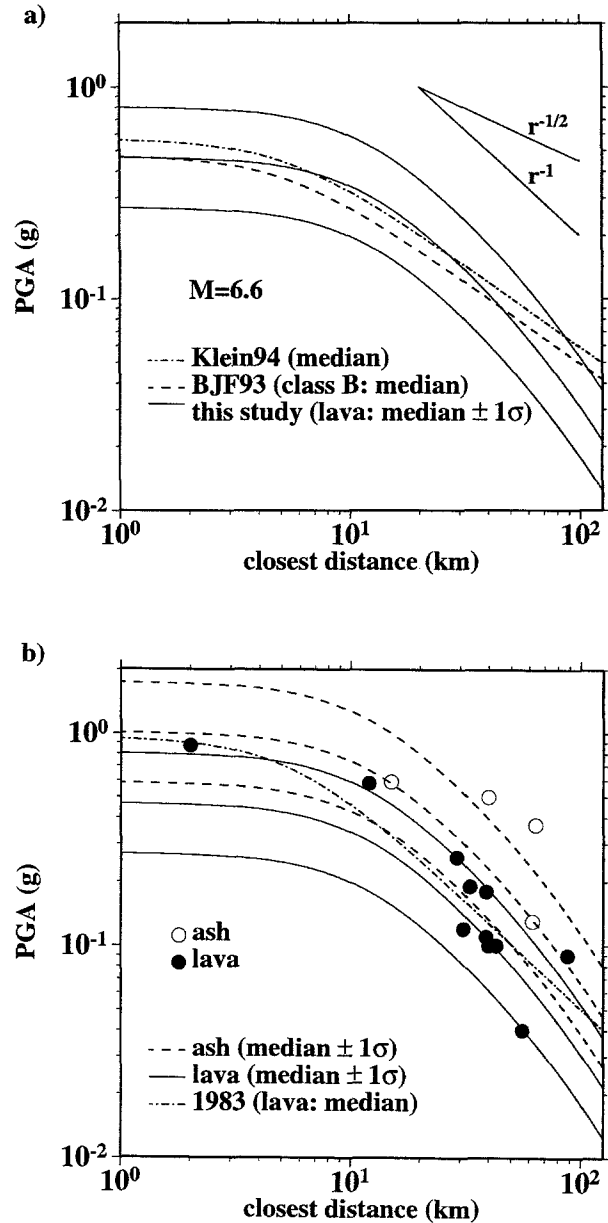

Figure 11. (a) Hawaii attenuation curve (lava, median, $\pm 1\sigma$), Boore *et al.* (1993) class B curve (dashed line), and Klein (1994) curve (dotted line). (b) Hawaii attenuation curve ($M = 6.6$) for lava (solid line) and ash (dashed line) site classifications (median, $\pm 1\sigma$) plotted with the 15 PGA values from the 1983 $M_s = 6.6$ Kaoiki earthquake and an attenuation curve derived from these same 15 PGA.

than 180 m/sec, respectively, in the upper 30 m. The site class C coefficient in the BJF93 attenuation relationship (0.254) is less than the ash site coefficient ($\hat{b}_4 = 0.335$) from our relationship; however, the ash site term represents accelerometer sites with S-wave velocities that vary from 60 to 200 m/sec. As such, a better comparison would be with the BJF93 site class D coefficient; however, site class D was
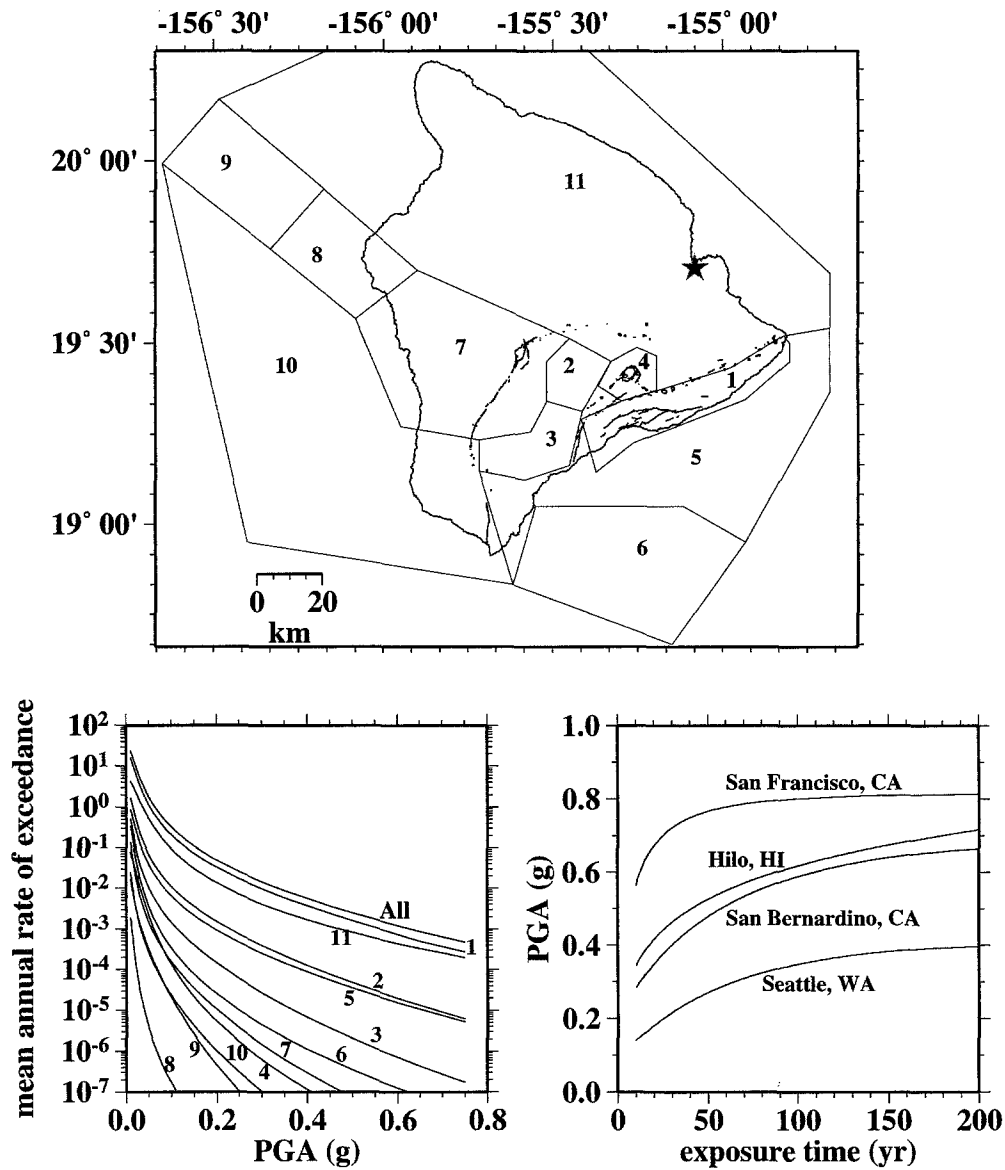
Figure 12.   (a) The 11 source zones used by Klein (1994) and (b) the resulting seismic hazard curves for Hilo (lava site) (c) PGA (rock) with 10% probability of exceedance versus exposure time for Hilo (this study); San Francisco, California; San Bernardino, California; and Seattle, Washington (NEHRP, 1993).

poorly represented in the data set and therefore not included in their analysis.

To evaluate the effect of the 15 PGA from the 1983 M_s = 6.6 Kaoiki earthquake on the attenuation relationship developed in this study, we determined a specific curve for the 1983 event using a shortened version of the Joyner and Boore two-stage regression method (cf. Cramer and Darragh, 1994). This curve (site coefficient $S = 0$) is shown in Figure 11b together with the 15 PGA from the Kaoiki earthquake and the full data set attenuation curve for lava and ash sites (median $\pm$ 1σ). As shown in Figure 11b, the attenuation rate of the 1983 Kaoiki relationship ($b_2 = 0$, $b_3 = -1.017$) is less than the full data set attenuation rate, and the Kaoiki relationship predicts substantially larger PGA at

distances less than 10 km due to the influence of the PGA of 0.87 g recorded at HVO1. The ash site coefficient for the Kaoiki attenuation relationship (0.429) is also larger than the full data set site coefficient reflecting the relatively large PGA recorded at the ash sites HIL5 and HON2.

Discussion

Hazards resulting from large earthquakes on the island of Hawaii include ground shaking, tsunamis, site amplification, landslides, secondary ground rupture, and triggered volcanic eruptions. An isoseismal map of the 1868 $M \approx 8$ great Kau earthquake shows maximum Modified Mercalli intensities ranging from X to XII over a large portion of the

southern part of the island (Wyss and Koyanagi, 1992). To compare the seismic hazards on the island of Hawaii to other locations in North America, we constructed a seismic hazard curve for Hilo, Hawaii. We developed this hazard curve using the 11 seismic source zones, recurrence values, and maximum magnitudes used by Klein (1994) together with the attenuation relationship developed in this study. Klein (1994) uses a maximum magnitude of either 7.5 or 7.7 for all of the source zones except zone 4, and although the magnitude range of the attenuation relationship developed in this study is from 4.0 to 7.2, the PGA predicted by our relationship for $M = 7.7$ and $d = 0$ km, 1.24 g, is very plausible given accounts of the ground motion from the 1868 great Kau earthquake (see Wyss and Koyanagi, 1992). Figure 12a shows the 11 source zones developed by Klein (1994) and Figure 12b shows the resulting seismic hazard curves for Hilo. Using the combined seismic hazard curve for Hilo, we then estimated PGA with a 10% probability of exceedance as a function of exposure time. Figure 12c shows PGA versus exposure time for Hilo and for San Francisco, California, San Bernardino, California, and Seattle, Washington, from a 1993 National Earthquake Hazards Reduction Program study (NEHRP, 1993). The PGA predicted for Hilo, Hawaii, are slightly larger than those for San Bernardino, California.

The seismic hazard curves we developed for Hilo are for a lava site. However, the results of this study and others show that a more significant hazard exists for structures located on ash deposits. The comparatively greater damage to structures built on ash deposits from enhanced ground motion in addition to the significant ash site coefficient in the Hawaii attenuation relationship indicates a need for additional ash sites in the Hawaii strong-motion network and further investigations of the geotechnical and seismic properties at each site. Reiter (1990) points out that when soil layers are thin, the amplification caused by the low soil impedance overpowers the loss in amplitude caused by soil damping. In addition, resonance can occur at, or close to, those high frequencies usually associated with peak accelerations. Site resonance and amplification are present on a number of Hawaii strong-motion accelerograms recorded on ash deposits.

Conclusions

We have developed an attenuation relationship by applying the Joyner and Boore two-stage regression method to the Hawaii PGA data set. We used this regression method in order to facilitate a comparison to a previous attenuation relationship used for Hawaii. The larger attenuation rate observed by this study for the island of Hawaii is due to a highly fractured volcanic pile that is less capable of transmitting the higher-frequency ground motion generally associated with peak ground accelerations. A plot of PGA with a 10% probability of exceedance for various exposure times shows that the seismic hazard for Hilo, Hawaii, is comparable to that for San Bernardino, California. As more earth-

quakes are recorded by the Hawaii strong-motion network, it will be possible to evaluate the attenuation rate for lower-frequency ground motion by estimating pseudo-velocity response spectra as a function of magnitude, distance, and site classification. The results of our study also show that site geology has a significant effect on PGA on Hawaii. This effect is characterized by large high-frequency reverberations in the thin ash layers that cover large portions of the island.

References

Ando, M. (1979). The Hawaii earthquake of November 29, 1975: Low dip angle faulting due to forceful injection of magma, _J. Geophys. Res._ **84,** 7616–7626.

Boore, D. M., W. B. Joyner, and T. E. Fumal (1993). Estimation of response spectra and peak accelerations from western North American earthquake: an interim report, _U.S. Geol. Surv. Open-File Rept. 93-509,_ 72 pp.

Bryan, C. J. (1992). A possible triggering mechanism for large Hawaiian earthquakes derived from an analysis of the 26 June 1989 Kilauea south flank sequence, _Bull. Seism. Soc. Am._ **82,** 2368–2390.

Buchanan-Banks, J. M. (1983). Reconnaissance map showing thickness of volcanic ash deposits in the greater Hilo area, Hawaii. U.S. Geol. Surv. Misc. Field Study Map MF-1449, scale 1:24,000.

Buchanan-Banks, J. M. (1987). Structural damage and ground failures from the November 16, 1983 Kaoiki earthquake, island of Hawaii, _U.S. Geol. Surv. Profess. Pap. 1350,_ 1187–1220.

Chiu, N. L., W. B. Lum, N. N. Nielson, and R. Y. Koyangi (1984). Damage survey of the Kaoiki, Hawaii earthquake of November 16, 1983, _Earthquake Spectra_ **1,** 173–195.

Cramer, C. H. and R. B. Darragh (1994). Peak accelerations from the 1992 Landers and Big Bear, California, Earthquakes, _Bull. Seism. Soc. Am._ **84,** 589–595.

Crosson, R. S. and E. T. Endo (1982). Focal mechanisms and locations of earthquakes in the vicinity of the 1975 Kalapana earthquake aftershock zone 1970–1979, _Tectonics_ **1,** 495–542.

Draper, N. R. and H. Smith (1981). _Applied Regression Analysis,_ 2nd ed., Wiley, New York, 709 pp.

Dvorak, J. J., A. T. Okamura, T. T. English, R. Y. Koyanagi, J. S. Nakata, M. K. Sato, W. T. Tanigawa, and K. M. Yamashita (1986). Mechanical response of the south flank of Kilauea Volcano, Hawaii, to intrusive events along the rift systems, _Tectonophysics_ **124,** 193–209.

Endo, E. T. (1985). Seismotectonic framework for the southeast flank of Mauna Loa volcano, Hawaii, _Ph.D. Thesis,_ University of Washington, Seattle, 349 pp.

Hanks, T. C. and H. Kanamori (1979). A moment magnitude scale, _J. Geophys. Res._ **84,** 2348–2350.

Harvey, D. and M. Wyss (1986). Comparison of a complex rupture model

with the precursor asperities of the 1975 Hawaii $M_s = 7.2$ earthquake, *Pure Appl. Geophys.* **124**, 957–973.

Hudson, D. E. (1979). *Reading and Interpreting Strong Motion Accelerograms*, Earthquake Engineering Research Institute Monograph, 112 pp.

Jackson, M. D., E. T. Endo, P. T. Delaney, T. Arnadottir, and A. M. Rubin (1992). Ground ruptures of the 1974 and 1983 Kaoiki earthquakes, Mauna Loa Volcano, Hawaii, *J. Geophys. Res.* **97**, 8775–8796.

Joyner, W. B. and D. M. Boore (1981). Peak horizontal acceleration and velocity from strong-motion records including records from the 1979 Imperial Valley, California, earthquake, *Bull. Seism. Soc. Am.* **71**, 2011–2038.

Joyner, W. B. and D. M. Boore (1993). Methods for regression analysis of strong-motion data, *Bull. Seism. Soc. Am.* **83**, 469–487.

Joyner, W. B. and D. M. Boore (1994). Errata, *Bull. Seism. Soc. Am.* **84**, 955–956.

Klein, F. W. (1994). Seismic hazards at Kilauea and Mauna Loa Volcanoes, Hawaii, *U.S. Geol. Surv. Open-File Rept. 94-216*, 96 pp.

Klein, F. W. and R. Y. Koyanagi (1989). The seismicity and tectonics of Hawaii, in *The Eastern Pacific Ocean and Hawaii*, J. Winterer, D. Hussong, and R. Decker (Editors), Geological Society of America, Boulder, Colorado, 238–252.

Koyanagi, R. Y., E. T. Endo, W. R. Tanigawa, J. S. Nakata, A. H. Tomori, and P. N. Tamura (1984). Kaoiki, Hawaii earthquake of November 16, 1983: a preliminary compilation of seismographic data at the Hawaii Volcano Observatory, *U.S. Geol. Surv. Open-File Rept. 84-798*, 34 pp.

Koyanagi, R. Y., C. J. Bryan, C. E. Johnson, J. S. Nakata, and W. R. Tanigawa (1989). Preliminary evaluation of the 6.1-magnitude Hawaii earthquake of June 25, 1989 and aftershocks, *EOS* **70**, 1409–1410.

Luetgert, J. H. (1992). MacRay: interactive two-dimensional seismic ray-tracing for the Macintosh, *U.S. Geol. Surv. Open-File Rept. 92-356*, 43 pp.

NEHRP (1993). *Building for the Future*, Fiscal Years 1991–1992 Report to Congress, National Earthquake Hazard Reduction Program, Washington, D.C., 123 pp.

Nielson, N. N., A. S. Furumoto, W. B. Lum, and B. J. Morrill (1977). The Honomu, Hawaii, earthquake: report of inspection, Washington, D.C., Natl. Acad. Sci., 79 pp.

Porcella, R. L. (1983). Seismic engineering program report, September–December 1980, *U.S. Geol. Surv. Circ. 854-C*, 19 pp.

Reiter, L. (1990). *Earthquake Hazard Analysis—Issues and Insights*, Columbia Univ. Press, New York, 254 pp.

Rubin, M., L. K. Gargulinski, and J. P. McGeehin (1987). Hawaiian radiocarbon dates, *U.S. Geol. Surv. Profess. Pap. 1350*, 209–213.

Savage, M. K. (1987). Spectral properties of Hawaiian microearthquakes: source, site, and attenuation effects, *Ph.D. Thesis*, University of Wisconsin-Madison, 209 pp.

Scherbaum, F. and M. Wyss (1990). Distribution of attenuation in the Kaoiki, Hawaii, source volume estimated by inversion of P wave spectra, *J. Geophys. Res.* **95**, 12439–12448.

Snedecor, G. W. and W. G. Cochran (1994). *Statistical Methods*, 8th ed., Iowa State Univ. Press, Ames, Iowa, 503 pp.

Tilling, R. I., R. Y. Koyanagi, P. W. Lipman, J. P. Lockwood, J. G. Moore, and D. A. Swanson (1976). Earthquake and related catastrophic events, Island of Hawaii, November 29, 1975: a preliminary report, *U.S. Geol. Surv. Circ. 740*, 33 pp.

Tomori, A. H., J. S. Nakata, P. G. Okubo, W. R. Tanigawa, and J. P. Tokuuke (1991). Hawaiian Volcano Observatory summary 90 part 1, seismic data, January to December 1990, *U.S. Geol. Surv. Open-File Rept. 91-578*, 79 pp.

Wieczorek, G. F., R. W. Jibson, R. C. Wilson, and J. M. Buchanan-Banks (1982). Geotechnical properties of ash deposits near Hilo, Hawaii, *U.S. Geol. Surv. Open-File Rept. 82-279*, 20 pp.

Wyss, M. and R. Y. Koyanagi (1992). Isoseismal maps, macroseismic epicenters and estimated magnitudes of historic earthquakes in the Hawaiian Islands, *U.S. Geol. Surv. Bull. 2006*, 93 pp.

Department of Geology and Geophysics
University of Wisconsin
Madison, Wisconsin 53706
E-mail: cgm1@nrc.gov and thurber@geology.wisc.edu